Analysis of the kinetic energy recovery behind a tidal stream turbine for various submergence levels

Pablo Ouro, Peter K. Stansby and Tim Stallard

Abstract—**Tidal turbines are commonly deployed at sea sites with water depths of up to 50 m to ease their deployment and quick maintenance operations. In these relatively shallow water depth conditions, the vertical expansion of tidal stream turbine wakes is restricted by the proximity of the rotor blades to the bottom bed and free-surface layer. These physical constrains can lead to changes in the flow mechanisms that drive momentum recovery behind the turbines, e.g. limiting the vertical fluxes of velocity. Understanding how the wake recovers depending on the submergence ratio is of utmost importance to designing the future multi-row tidal turbine arrays. Here, we adopt high-fidelity Large-Eddy Simulations (LES) with an Actuator Line Method (ALM) to represent the turbine's rotor to analyse the mean flow and transport equation for mean kinetic energy (MKE) behind a single bottom-fixed tidal turbine for four water depth values. Our results show that the close proximity of the turbine blade tip to the free-surface can notably constrain the wake expansion, with very shallow conditions leading to a limited contribution to the MKE replenishment of the turbulent momentum exchange over the vertical direction. Conversely, under such shallow conditions, the horizontal flux of MKE is enhanced over the lateral boundaries of the downstream wake. Our study evidences that the ratio of water depth to turbine diameter plays a relevant role in future tidal arrays and needs to be correctly accounted for in numerical models to provide reliable results.**

Index Terms—**Large-eddy simulation, mean kinetic energy, tidal stream energy, tidal turbine, wake recovery.**

Paper submitted on 22 Dec. 2021; published 19 December 2022.

Work supported by the Supercomputing Wales project, which is part-funded by the European Regional Development Fund (ERDF) via the Welsh Government. Part of the presented material has been supported by the Dame Kathleen Ollerenshaw Fellowship that Pablo Ouro holds at the University of Manchester, and by the Tidal Stream Industry Energiser (TIGER), co-financed by the ERDF through the Interreg France (Channel) England Programme

Pablo Ouro. Dame Kathleen Ollerenshaw Research Fellow. School of Mechanical, Aerospace and Civil Engineering, University of Manchester, Manchester, M13 9PL, UK (e-mail: pablo.ouro@manchester.ac.uk).

Peter K. Stansby. Professor of Hydrodynamics. School of Mechanical, Aerospace and Civil Engineering, University of Manchester, Manchester, M13 9PL, UK (e-mail: peter.stansby@manchester.ac.uk).

Tim Stallard. Professor of Offshore & Renewable Energy Engineering. School of Mechanical, Aerospace and Civil Engineering, University of Manchester, Manchester, M13 9PL, UK (e-mail: tim.stallard@manchester.ac.uk).

Digital Object Identifier: https://doi.org/10.36688/imej.5.265-272

I. Introduction

The size and number of arrays of tidal stream turbines to be deployed worldwide is expected to notably increase over the next years, especially in the UK, Canada and France in which the tidal resource is high. Most of the identified deployment sites have relatively shallow conditions as these enable quicker and easier maintenance operations that reduce the levelised cost of energy, whilst other design considerations are required to be considered such as keeping a minimum clearance between the turbine rotor blades top tips and minimum water depth in order to avoid interactions with navigating vessels. However, deploying tidal stream turbines in such vertically confined environments can change the flow mechanisms that govern the wake evolution and recovery, which will be of utmost importance in multi-row tidal arrays as an internal boundary layer can be developed due to the turbines interacting with the approaching flow, similarly to offshore wind farm flows [1].

The main flow structures generated downstream of a tidal turbine, e.g. tip and hub vortices, have been extensively studied through experiments [2] and high-fidelity numerical simulations [3]–[5] which have also investigated the wake recovery rate for different ambient turbulent flow conditions, e.g. turbulence intensity and length scales [6]–[8]. However, in tidal turbine arrays the complexity of the generated flow field increases due to turbine-to-turbine interactions. The turbines are located in rows relatively close one another and hence devices in secondary rows are prone to be negatively affected by the low-momentum turbulent wake originated from the upstream devices. This leads a reduction in their energy generation capabilities and triggering loading oscillations that poses a structural challenge both in terms of the maximum loads and fatigue loadings [6], [9]. Thus the efficient design of arrays of tidal stream turbines depends on minimising the inter-play between the devices placed in different rows, requiring a deep understanding of the three-dimensional turbulent flow developed behind each individual turbine under realistic environmental flow conditions, i.e. including uneven bathymetry, water depth constrains in shallow conditions, and wave action.

To date, most of the undertaken research has considered uniform flat bed conditions neglecting bathymetry-induced turbulence, which can increase

the wake recovery rate due to an enhanced turbulent transport [10]–[12], and how the proximity of the turbine's blade tips to the free-surface might impact the wake recovery [13]. These physical constraints can impact the wake structure and energy generation capabilities of secondary rows in large tidal turbine arrays, thus need to be carefully studied to best design future arrays, e.g. optimal inter-row spacing, and develop more suitable low-order wake models. Such investigation of the environmental conditions on tidal array flow is analogous to the developments in offshore wind energy over the last years, in which a better understanding of the wake expansion and redistribution of mean kinetic energy has proven essential to optimally design offshore wind farms. Note that the flow within tidal and wind turbine arrays differ mainly due to the latter operating in the atmospheric boundary layer that is only constrained by the ground surface but not upwards [1] while in the marine environment there are two horizontal layers, namely the bottom bed and the free-surface [14].

In this paper, we perform high-fidelity large-eddy simulations using the Digital Offshore FArms Simulator (DOFAS) to analyse the wake evolution and recovery of the kinetic energy of the mean flow for a single tidal stream turbine under four different relative submergences. We aim to inform how the clearance between the turbine top-tip height and free-surface level impacts the wake evolution to finally assess over which threshold such effect is minimal.

II. Numerical framework

The state-of-the-art DOFAS (Digital Offshore Farms Simulator) [9] is adopted to perform high-fidelity Large-Eddy Simulation (LES) by solving the spatially-filtered Navier-Stokes equations. LES allows the resolution of the turbulent scales larger than the grid size which enables to quantify the contribution from the turbulent stresses to the kinetic energy recovery over the turbine's wake region in an accurate manner.

In DOFAS, simulations are advanced in time using a pressure-correction fractional-step method, with a three-step low-storage Runge-Kutta method to compute the advective and diffusive fluxes. The spatial domain is discretised with a rectangular Cartesian grid with staggered storage of velocities and partitioned in sub-domains whose communication is performed using an Message Passing Interface (MPI) protocol to effectively run the simulations in parallel. The unresolved subgrid scale stresses are approximated by the Wall-Adapting Local Eddy-viscosity (WALE) sub-grid scale (sgs) model [15], [16].

DOFAS uses an Actuator Line Method (ALM) with a tip-loss correction term to represent the turbine rotor blades [17], [18], an Immersed Boundary Method (IBM) to represent static or dynamic solid bodies such as the turbine nacelles and support structures [8], [11] and artificial turbulent inflow conditions can be generated using an anisotropic Synthetic Eddy Method (SEM) [19]. From hereafter, we adopt $\langle . \rangle$ to refer to temporal averaging operation and $.'$ to indicate turbulent fluctuations.

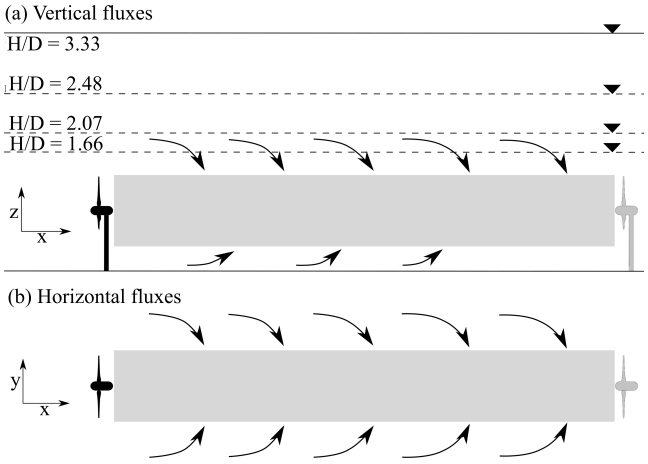

Fig. 1. Turbine wake region (shadowed in grey) used to integrate the mean kinetic energy equation terms. Representation of the fluxes in the (a) vertical and (b) lateral directions. Flow is from left to right.

The dynamics of the mean-flow energy are analysed with the transport equation for the Mean Kinetic Energy (MKE), also defined as $K = \frac{1}{2}\langle u_i \rangle^2$, which is obtained by multiplying the spatially-filtered momentum equation for mean velocities by the time-averaged streamwise velocity component $\langle u_i \rangle$, and reads:

$$
\begin{aligned}
0 = & \overbrace{-\langle u_j \rangle \frac{\partial K}{\partial x_j}}^{I} \quad \overbrace{-\langle u_i \rangle \frac{1}{\rho} \frac{\partial \langle p \rangle}{\partial x_i}}^{II} \\
& + \overbrace{\frac{\partial}{\partial x_j}\left(\nu \langle u_i \rangle \frac{\partial \langle u_i \rangle}{\partial x_j} \right)}^{III} \quad \overbrace{-\frac{\partial \left(\langle u_i \rangle \langle u_i' u_j' \rangle \right)}{\partial x_j}}^{IV} \\
& \underbrace{-\langle u_i' u_j' \rangle \frac{\partial \langle u_i \rangle}{\partial x_j}}_{V} \quad \underbrace{-\nu \left(\frac{\partial \langle u_i \rangle}{\partial x_j} \right)^2}_{VI} \quad \underbrace{+ \frac{1}{\rho} \langle u_i \rangle f_i}_{VII}
\end{aligned}
\tag{1}
$$

Here $\langle p \rangle$ denotes time-averaged pressure values, x_i and x_j indicate the spatial direction (i, j = 1,2,3), ρ is the density of the fluid, ν is the kinematic viscosity of the fluid, f_i is a source term representing the forces exerted by the ALM or IBM, and $\langle u_i' u_j' \rangle$ are the time-averaged turbulent fluctuation correlations that result from summing the Reynolds and sub-grid scale stresses.

We evaluate each term in the budget equation for K to identify the flow mechanisms that mainly contribute to its replenishment, loss and transport over the turbine wake region depicted in Figure 1 that extends up to 13 diameters downstream of the device. These terms of Eq. 1 are integrated in the streamwise distance over the lateral and vertical directions (yz-plane) in an area that extends 1.1 diameters centred with the turbine's rotor, as presented in Figure 1, in order to include the shear layers developed in the outer region of the wake [9]. The meaning of the terms involved in the K equation (Eq. 1) is:

- I represents the advection of mean kinetic energy,
- II is the mechanical work produced by gradients in the mean pressure field,
- III is the work done by the viscous stresses,
- IV is the work done by the turbulent stresses, representing the transport by Reynolds stresses,

- V is the work of deformation by turbulence stresses,
- VI is the viscous dissipation,
- VII is the power extracted by the turbine.

Note that the production term V ($\langle u_i' u_j' \rangle \partial \langle u_i \rangle / \partial x_j$, Eq. 1) has a negative sign denoting a negative contribution (or "dissipation") of MKE in the flow that can be interpreted as the rate at which K is lost from the mean flow and transferred to the turbulent eddies, i.e. denotes the generation of turbulent kinetic energy from turbulent shear production. The production term in the vertical direction ($-\langle u'w' \rangle \partial \langle u \rangle / \partial z$) has special importance in the present study as it is likely to be impacted by the clearance between the turbine's blade top tip location to the free-surface layer. Furthermore, in our analysis the viscous terms III and VI are neglected due to the relatively high Reynolds number of the flows considered, and the term VII corresponding to the forces from the ALM and IBM is also discarded as the turbines are not embedded into the integrated wake region (see Figure 1).

III. Test cases

The laboratory-scale tidal stream turbine from Stallard et al. [2] is considered in this work, as DOFAS has previously been validated in the prediction of the mean velocity field developed in two-row arrays deployed in the same experimental facility [20] and under identical flow conditions [9]. A depth-averaged velocity (U_0) of 0.47 m s^{-1} was found in the experimental tests with streamwise velocities following a smooth logarithmic distribution with a friction velocity (u_*) equal to 0.0167 m s^{-1}, and the water depth was kept uniform with a value of H = 0.45 m. The turbine has a diameter (D) of 0.27 m with the rotor centre located at mid depth, operating according to the optimal tip-speed ratio of 4.5 that results in a fixed rotational speed of 15.33 rad s^{-1}.

In the experimental setup [2], the depth-to-diameter (H/D) ratio was small with a value of 1.66. To investigate the effect of relative submergence on the wake recovery, we simulated with DOFAS four different water depths, namely 0.45 m, 0.56 m, 0.67 m, and 0.90 m, that provided values H/D of 1.66, 2.07, 2.48 and 3.33, respectively. In the experiments the supporting vertical cylinder was placed above the hub and piercing the water surface to connect the turbine's hub to the overlaying support structure located above the free-surface. In our LESs, the turbines are bottom-fixed with the turbine's rotor height kept at the same distance of 0.225 m over the flume bottom but with the vertical supporting structure placed underneath the hub connecting it to the flume's bed so it remains unchanged irrespective of the water depth value.

The computational domain extends over 11.0 m in the streamwise direction and 5.4 m in the lateral direction with the simulations running on Supercomputing Wales facilities with 51 CPUs for the case with H = 0.45 m and on 102 CPUs for the deeper water depths. A uniform mesh resolution of 0.005 m in the three spatial directions and fixed time step of 0.001 s are adopted as in previous studies these provided accurate results of flow statistics and turbine's hydrodynamic coefficients [18]. Simulations are run for 250 s in total, i.e. approx. 600 revolutions, with mean velocities being computed after 50 s and second order statistics after 80 s once the first order statistics are deemed converged.

Regarding the boundary conditions, at the inlet a Dirichlet boundary condition is imposed following the logarithmic velocity profile measured in the experiments and superimposing artificial turbulent fluctuations with an anisotropic Synthetic Eddy Method (SEM) set according the turbulence length scales and intensity reported in the experimental work [20]. A smooth-bed wall function is adopted at the bottom and lateral walls of the flume, whilst the free-surface layer is treated as a shear-free rigid-lid boundary condition. A Neumann boundary condition is adopted at the outlet of the domain.

IV. Results

The distribution of the mean streamwise velocity field ($\langle u \rangle / U_0$) for the four submergence cases is presented in Figure 2 with xz-vertical planes laterally averaged in the y-direction and the origin of streamwise coordinates (x/D = 0) set at the turbines' rotor plane location. The low-momentum wake behind the turbine is almost identical between cases in terms of spatial distribution and velocity magnitude. This is also observed in Figure 3 with vertical profiles of $\langle u \rangle / U_0$ at x/D = 2, 4, 8 and 12. For the shallowest condition (as the one in the experiments), the flow overtopping the rotor (between blade top tip height and free-surface level) experiences a larger acceleration until approx. x/D = 2.0 in comparison to the other cases, and also features slightly larger velocities at z/D = 0.2. At x/D = 4.0, the vertical profiles in all submergence levels are nearly identical, whilst from $x/D \geq 8$ with H/D = 1.66 there is a flow deceleration at elevations closer to the free-surface that is not observed in the cases with deeper water depths. Overall, for submergence ratios larger than 2.07 there is no significant change in the mean streamwise velocity distribution throught the wake.

Figure 3 also presents the vertical distribution of the spanwise-averaged streamwise turbulence intensity ($\langle u' \rangle / U_0$, with $\langle u' \rangle = \langle u'u' \rangle^{0.5}$) and vertical Reynolds shear stresses ($-\langle u'w' \rangle / u_*^2$). The turbulence intensity at x/D = 2 is very similar amongst the analysed cases as it lies in the near-wake region in which the flow is dominated by the turbine's action. At x/D = 4, the peak in turbulence intensity below the hub height, i.e. at $z/D \leq 0.8315$, has a higher maximum for the shallowest submergence compared to the other conditions. In the far-wake, at downstream distances of $8D$ and $12D$, the vertical distribution of $\langle u' \rangle$ attains its maxima near the top and bottom tip locations (z/D = 1.333 and 0.333, respectively) with the minimum at hub height.

Tip vortices generated by the rotating turbine blades generate a turbulent shear layer characterised by large shear stresses due to the turbulent momentum exchange, which are well observed in the vertical contours of Reynolds shear stresses in Figure 4 and vertical

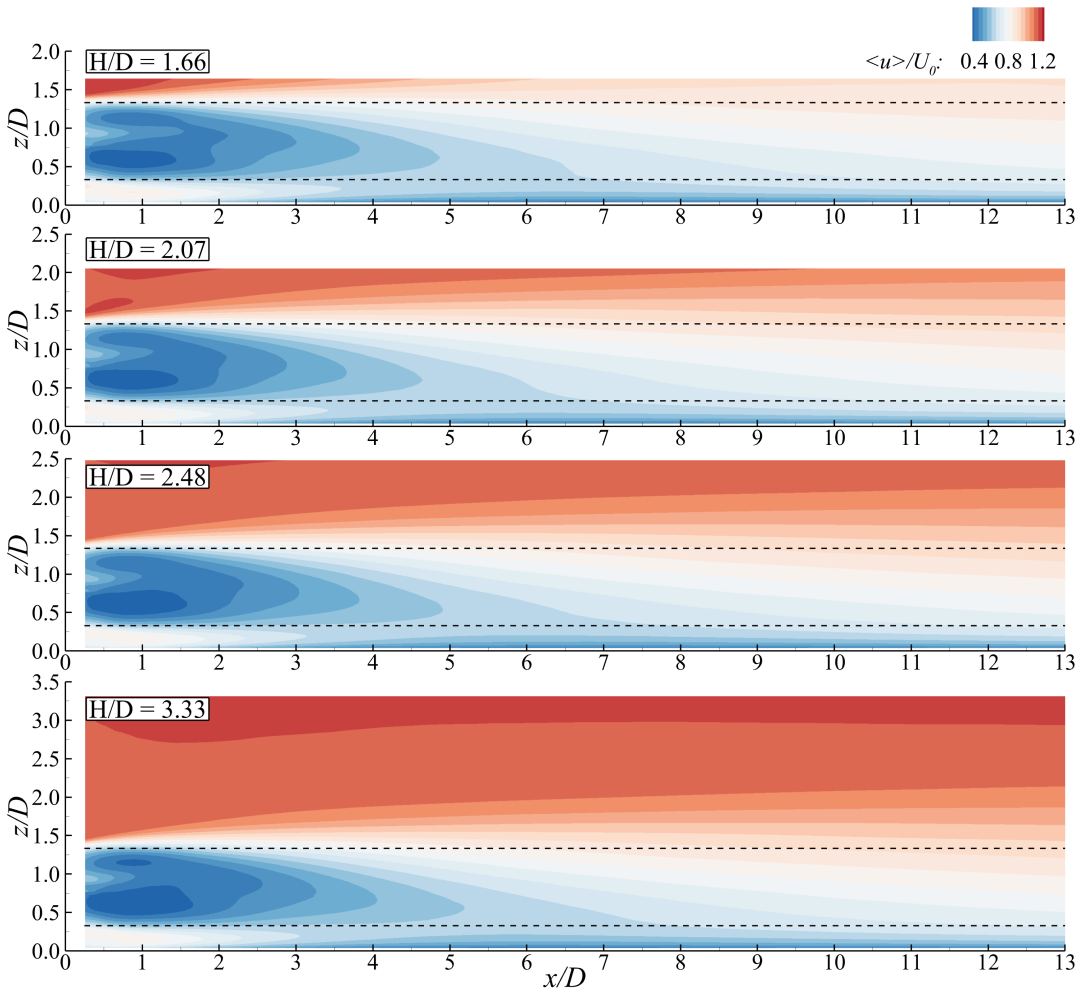

Fig. 2. Distribution of mean velocities over vertical planes for the four submergence cases. Results are averaged over the lateral wake region indicated in Figure 1. Turbine rotor are located at x/D = 0.0.

profiles at x/D = 2, 4, 8 and 12 in Figure 3. Irrespective of the relative submergence, the top shear layer extends vertically up to $z/D \approx 2.0$ with almost identical values for the cases with H/D = 2.48 and 3.33. However, this shear layer is notably constrained for the shallower cases, especially for H/D = 1.66 in which the peak value of $-\langle u'w' \rangle / u_*^2$ is constantly lower throughout the wake length. The upper shear layer features higher absolute values than the bottom one (see Figure 3c) as the approaching flow at such height is faster, thus enhancing the turbulent momentum exchange. Conversely, the bottom shear layer appears unchanged regardless the submergence. Our result show that for $H/D \geq 2.48$ the distribution of the vertical shear stresses remains the same, with a high turbulent momentum exchange observed until distances of approx. $12D$ downstream of the turbine with maxima consistently found at top tip height.

Further insigths into the impact of proximity of the turbine to the free-surface are provided in Figure 5 with contours of mean relative pressure ($\langle p \rangle$), which can be deemed as a proxy for free-surface deformation [21]. Only for the H/D = 1.66 case there are possitive values of relative pressure upstream of the turbine (indicating a potential rise in water depth) which rapidly transition to negative values immediately downstream. For the larger submergence cases there is also a similar transition in the pressure field but with lower values which, together with the already larger water depth value, indicates that relative free-surface effects for cases with $H/D \geq 2.0$ might not relevant.

We further analyse the distribution of the relevant terms in the mean kinetic energy (MKE) equation (Eq. 1), namely convection of MKE, work due to the pressure gradient, transport from turbulent stresses, and production of turbulent kinetic energy, over the streamwise direction with results averaged over yz-planes in the cross-section extending $-0.55D \leq y, z \leq 0.55D$ shown in Fig. 1. Results are provided in Figure 6 for the four submergence cases with value of each component in the x-, y- and z-directions except for the pressure term.

The transport of MKE due to convection in the streamwise direction and work from the pressure gradients over the wake appears to be counterbalanced by the turbulent transport terms and also lateral and vertical convection ones. The pressure gradient term attains increasing values as the water depth decreases due to the higher blockage caused by the turbine in the flow, whilst the opposite is found for the streamwise convection term. The role of the terms related to the destruction of MKE or production of tke are

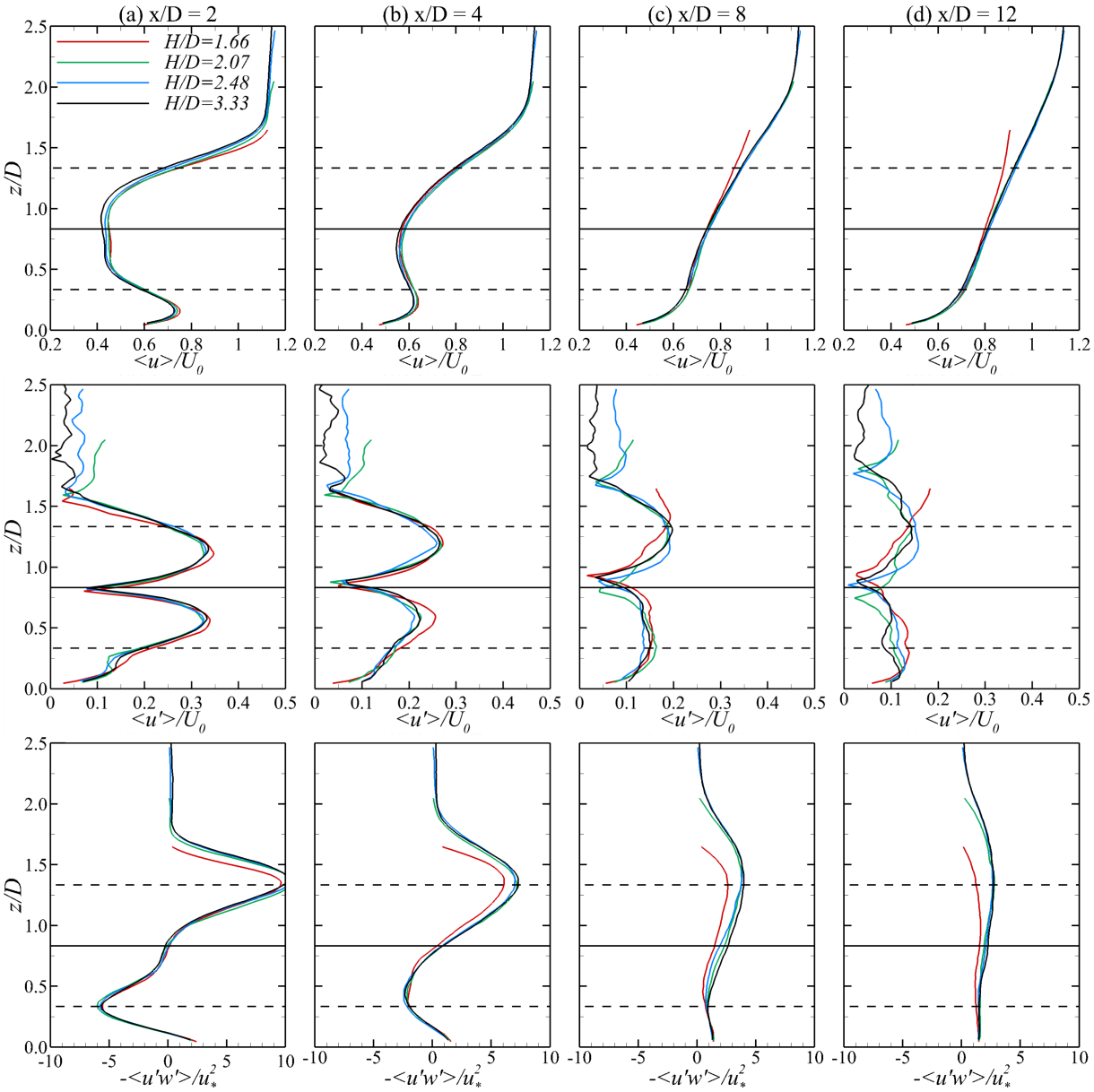

Fig. 3. Vertical distribution of mean (a) streamwise velocities, (b) turbulence intensity and (c) vertical Reynolds shear stresses for the four submergence cases. Results are averaged over the lateral wake region indicated in Figure 1.

largest in the near wake until $x/D \approx 6$ irrespective of the water depth level. In the far wake region, the overall contribution from the turbulent transport terms is balanced by the pressure gradient and streamwise convection terms. Our results agree qualitatively with those found by Yang et al. [22] for a single wind turbine operating behind a hill but in our cases the work from the pressure gradients play a more important role likely due to the vertically constrained environment of tidal flows.

Noticeable differences in the distribution of the turbulent transport components are found for the shallowest case (H/D = 1.66) in comparison to the deeper submergence setups, as the vertical turbulent transport of MKE is reduced after x/D = 2 and becoming almost negligible after x/D = 10, and accompanied by an enhanced turbulent transport in the y-direction after x/D = 5. A similar distribution is found for the y- and z-components of the MKE convection for H/D = 1.66. Finally, the present results suggest that the governing mechanisms driving MKE recovery remain fairly unchanged for relative submergences of H/D larger than 2.48.

V. Conclusion

Tidal stream turbines operate in highly constrained environments limited in the vertical direction by the bottom bed and free-surface layers, which affect the flow mechanisms governing the recovery and distribution of the mean kinetic energy in their wake. In this paper, we have performed large-eddy simulations using the state-of-the-art Digital Offshore FArms Simulator (DOFAS) to analyse the impact of the relative submerge on the wake evolution and momentum recovery behind a single tidal stream turbine. Our results show that the wake characteristics behind a single device are influenced when it operates in a relative submergence (H/D, with H being the water depth and D the diam-

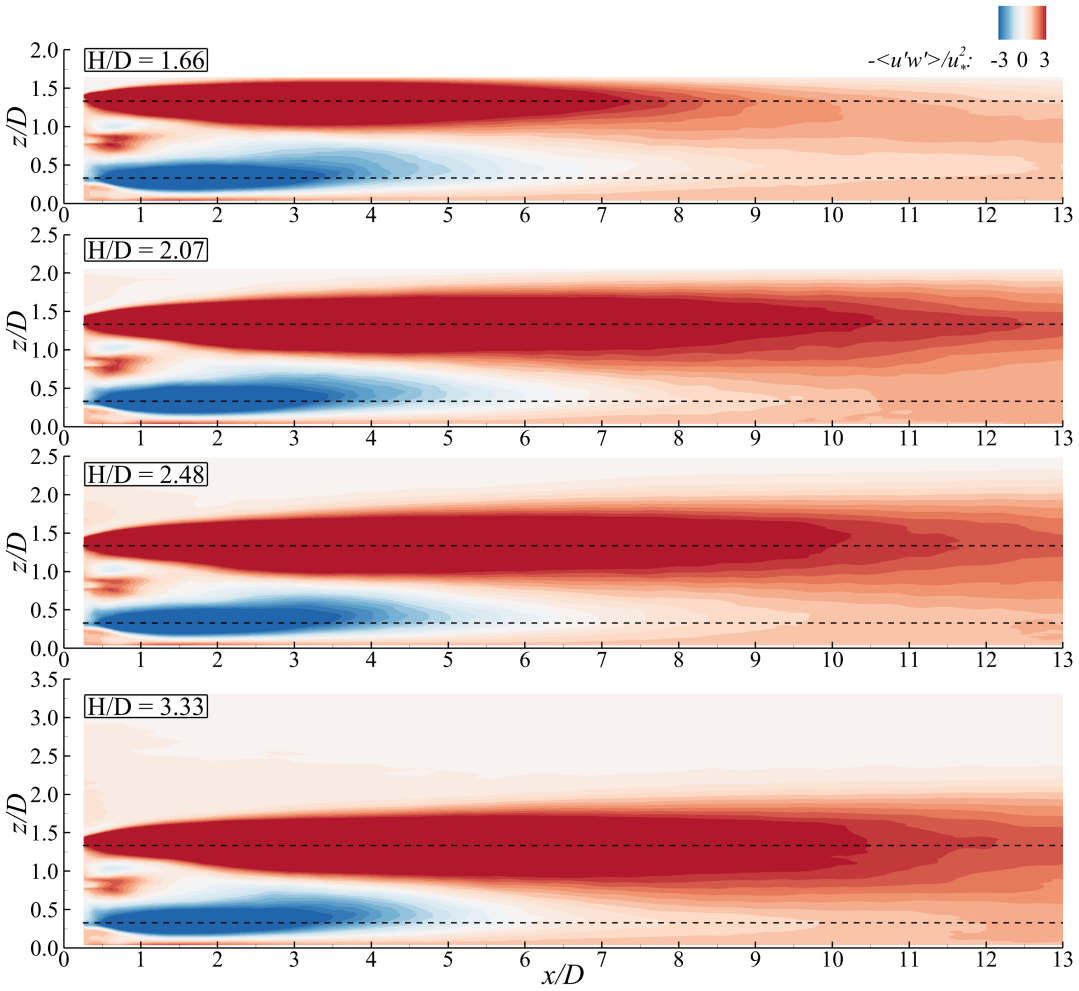

Fig. 4. Distribution of vertical shear stresses normalised by friction velocity ($-\langle u'w'\rangle/u_*^2$) over the xz vertical plane for the four submergence cases. Results are averaged over the lateral wake region, as indicated in Figure 1.

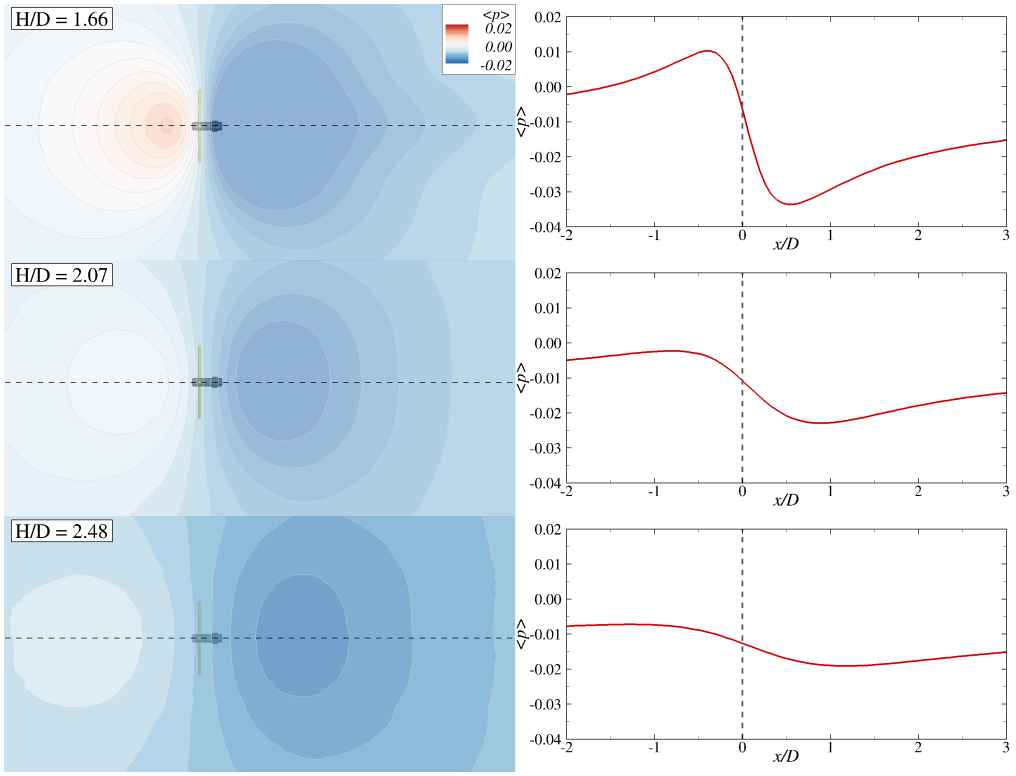

Fig. 5. Distribution of mean relative pressure at the top rigid-lid over the xy horizontal plane for the three submergence cases H/D = 1.66, 2.07 and 2.48. The distribution of relative pressure along the line at y/D = 0 are provided on the right hand side.

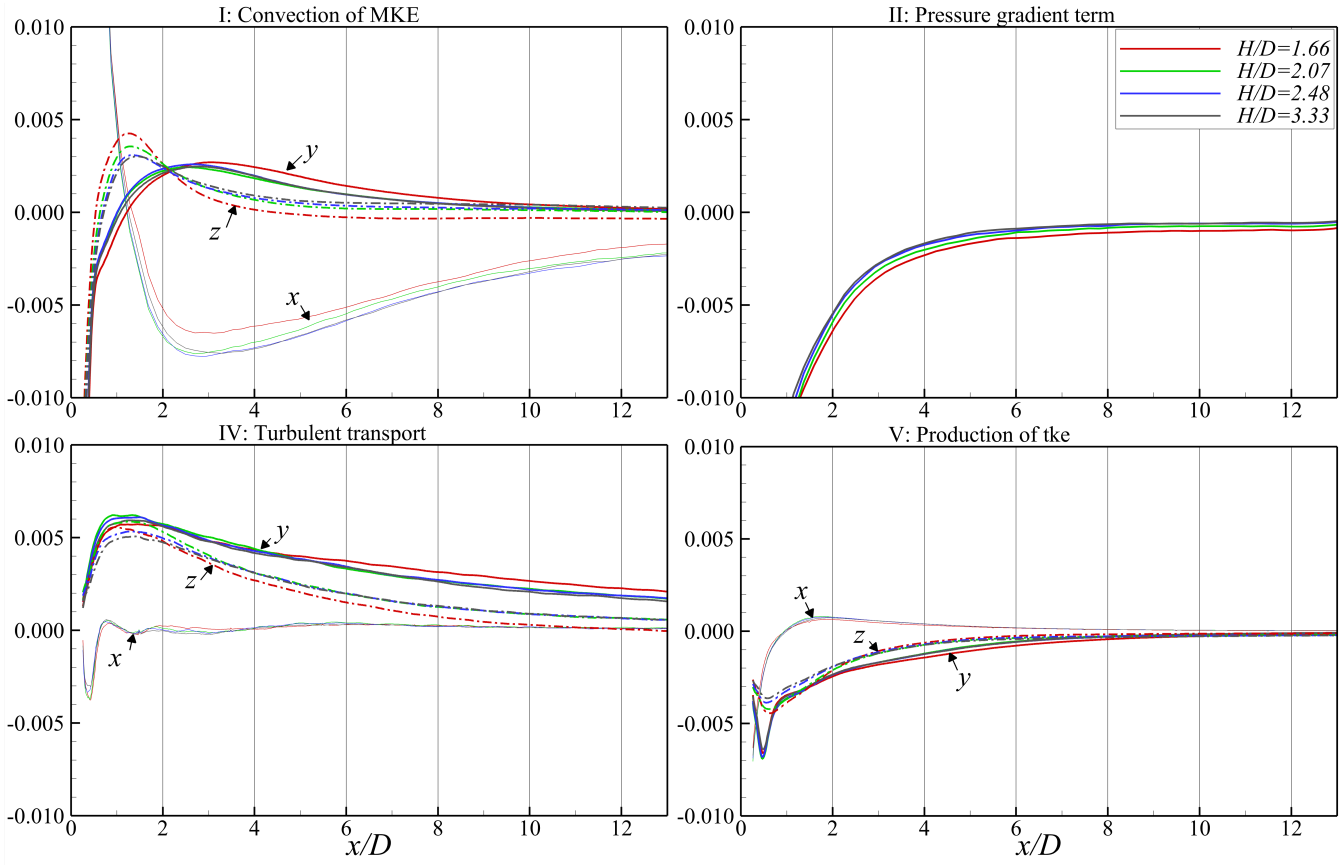

Fig. 6. Streamwise variation of the cross-sectional averaged value of mean kinetic energy equation terms (Eq. 1) in the wake region.

eter of the turbine) lower than approx. 2.0 due to the inability of the wake to expand vertically, thus limiting the vertical turbulent momentum exchange occurring in the upper shear layer induced by tip vortices.

The budget of mean kinetic energy equation indicated that the turbulent transport and convection terms in the lateral and vertical directions contributes positively to its replenishment over the entire wake, which are counter-balanced by the streamwise convection, work from the pressure gradient and production of turbulent kinetic energy. In the far-wake, after six to eight diameters downstream of the turbine, the turbulent transport is the only responsible for the replenish the kinetic energy of the mean flow balanced by the streamwise convection term and pressure gradient component.

Contours of mean pressure at the top boundary (rigid lid) suggest that free-surface effects might play a role for cases with $H/D \leq 2.0$ which can change the mechanisms driving the wake recovery. Such effects appear much reduced for the deeper submergence cases.

These findings have two important implications: firstly, in presence of irregular bathymetry or waves there is an enhanced vertical transport of turbulence and thus these can positively contribute to replenish the mean kinetic energy; and secondly, bathymetries with increasing (or decreasing) slope represent an adverse (or favourable) pressure gradient respectively, which can accelerate (or decelerate) wake recovery.

In spite of our results showed a reduced impact of the water depth on the mean velocity characteristics, further relevance is expected in large tidal turbine arrays in which an internal boundary layer with growing vertical extent is expected occur. Thus, our study provides enough evidences to outline that future tidal turbine arrays deployed in relatively shallow waters can experience a decreased energy generation capability in the secondary-row turbines due to the restrained wake recovery.

REFERENCES

[1] R. J. Stevens and C. Meneveau, "Flow Structure and Turbulence in Wind Farms," vol. 49, no. 1, pp. 311–339, 2017.

[2] T. Stallard, T. Feng, and P. K. Stansby, "Experimental study of the mean wake of a tidal stream rotor in a shallow turbulent flow," *Journal of Fluids and Structures*, vol. Accepted, 2022.

[3] I. Afgan, J. McNaughton, S. Rolfo, D. D. Apsley, T. Stallard, and P. Stansby, "Turbulent flow and loading on a tidal stream turbine by LES and RANS," *International Journal of Heat and Fluid Flow*, vol. 43, pp. 96–108, 2013.

[4] S. Kang, X. Yang, and F. Sotiropoulos, "On the onset of wake meandering for an axial flow turbine in a turbulent open channel flow," *Journal of Fluid Mechanics*, vol. 744, pp. 376–403, 2014.

[5] A. Posa and R. Broglia, "Characterization of the turbulent wake of an axial-flow hydrokinetic turbine via large-eddy simulation," *Computers and Fluids*, vol. 216, p. 104815, 2021.

[6] P. Mycek, B. Gaurier, G. Germain, G. Pinon, and E. Rivoalen, "Experimental study of the turbulence intensity effects on marine current turbines behaviour. Part I: One single turbine," *Renewable Energy*, vol. 66, pp. 729–746, 2014.

[7] T. Blackmore, L. E. Myers, and A. S. Bahaj, "Effects of turbulence on tidal turbines: Implications to performance, blade loads, and condition monitoring," *International Journal of Marine Energy*, vol. 14, pp. 1–26, 2016.

[8] P. Ouro, M. Harrold, T. Stoesser, and P. Bromley, "Hydrodynamic loadings on a horizontal axis tidal turbine prototype," *Journal of Fluids and Structures*, vol. 71, pp. 78–95, 2017.

[9] P. Ouro, L. Ramírez, and M. Harrold, "Analysis of array spacing on tidal stream turbine farm performance using Large-Eddy Simulation," *Journal of Fluids and Structures*, vol. 91, p. 102732, 2019.

[10] M. Musa, C. Hill, F. Sotiropoulos, and M. Guala, "Performance and resilience of hydrokinetic turbine arrays under large migrating fluvial bedforms," *Nature Energy*, vol. 3, pp. 839–846, 2018.

[11] P. Ouro and T. Stoesser, "Impact of Environmental Turbulence on the Performance and Loadings of a Tidal Stream Turbine," *Flow, Turbulence and Combustion*, vol. 102, no. 3, pp. 613–639, 2019.

[12] P. Mercier, M. Grondeau, S. Guillou, J. Thiébot, and E. Poizot, "Numerical study of the turbulent eddies generated by the seabed roughness. Case study at a tidal power site," *Applied Ocean Research*, vol. 97, p. 102082, 2020.

[13] P. Aghsaee and C. D. Markfort, "Effects of flow depth variations on the wake recovery behind a horizontal-axis hydrokinetic instream turbine," *Renewable Energy*, vol. 125, pp. 620–629, 2018.

[14] P. K. Stansby and P. Ouro, "Modelling marine turbine arrays in tidal flow," *Journal of Hydraulic Research*, 2022.

[15] F. Nicoud and F. Ducros, "Subgrid-scale stress modelling based on the square of the velocity gradient tensor," *Flow, Turbulence and Combustion*, vol. 62, no. 3, pp. 183–200, 1999.

[16] P. Ouro and T. Stoesser, "An immersed boundary-based large-eddy simulation approach to predict the performance of vertical axis tidal turbines," *Computers & Fluids*, vol. 152, pp. 74–87, 2017.

[17] W. Z. Shen, J. N. Sørensen, and R. Mikkelsen, "Tip Loss Correction for Actuator/Navier–Stokes Computations," *Journal of Solar Energy Engineering*, vol. 127, no. 2, pp. 209–213, 2005.

[18] P. Ouro, M. Harrold, L. Ramirez, and T. Stoesser, "Prediction of the Wake Behind a Horizontal Axis Tidal Turbine Using a LES-ALM," in *Progress in CFD for Wind and Tidal Offshore Turbines*. Springer, 2019, ch. 4, pp. 25–35.

[19] N. Jarrin, R. Prosser, J.-C. Uribe, S. Benhamadouche, and D. Laurence, "Reconstruction of turbulent fluctuations for hybrid RANS/LES simulations using a Synthetic-Eddy Method," *International Journal of Heat and Fluid Flow*, vol. 30, no. 3, pp. 435–442, 2009.

[20] T. Stallard, R. Collings, T. Feng, and J. Whelan, "Interactions between tidal turbine wakes: experimental study of a group of three-bladed rotors." *Philosophical transactions. Series A, Mathematical, physical, and engineering sciences*, vol. 371, p. 20120159, 2013.

[21] P. Ramos, L. Schindfessel, J. Pêgo, and T. De Mulder, "Flat vs. Curved rigid-lid LES computations of an open-channel confluence," *Journal of hydrodynamics*, vol. 21, pp. 318–334, 2019.

[22] X. Yang, K. B. Howard, M. Guala, and F. Sotiropoulos, "Effects of a three-dimensional hill on the wake characteristics of a model wind turbine," *Physics of Fluids*, vol. 27, no. 2, p. 025103, 2015.